Power law hopping of single particles in one-dimensional non-Hermitian quasicrystals

Dechi Peng, Shujie Cheng,* and Gao Xianlong †
Department of Physics, Zhejiang Normal University, Jinhua 321004, China

(Received 16 January 2023; accepted 2 May 2023; published 12 May 2023)

In this paper, a non-Hermitian Aubry-André-Harper model with power law hoppings ($1/s^a$) and quasiperiodic parameter β is studied, where a is the power law index, s is the hopping distance, and β is a member of the metallic mean family. We find that the number of the quasiperiodic parameter β-dependent regimes depends on the strength of the non-Hermiticity. Under a particularly weak non-Hermitian effect, there preserves $P_{\ell=1,2,3,4}$ regimes where the fraction of ergodic eigenstates is β dependent as $\beta^\ell L$ (L is the system size), similar to those in the Hermitian case. However, P_ℓ regimes are ruined by the strong non-Hermitian effect. Moreover, by analyzing the fractal dimension, we find that there are two types of edges aroused by the power law index a in the single-particle spectrum, i.e., an ergodic-to-multifractal edge for the long-range hopping case ($a < 1$), and an ergodic-to-localized edge for the short-range hopping case ($a > 1$). Meanwhile, the existence of these two types of edges is found to be robust against the non-Hermitian effect. By employing the Simon-Spence theory, we analyzed the absence of the localized states for $a < 1$. For the short-range hopping case, with the Avila's global theory and the Sarnak method, we consider a specific example with $a = 2$ to reveal the presence of the intermediate phase and to analytically locate the intermediate regime and the ergodic-to-localized edge, which are self-consistent with the numerically results.

DOI: 10.1103/PhysRevB.107.174205

I. INTRODUCTION

In 1958, P. W. Anderson pointed out that free particles will present localized behavior due to random disorders. The absence of diffusion is known as Anderson localization [1]. The scaling theory shows [2–4] that systems change from the fully ergodic phase to fully the localized phase with the arbitrarily weak disorder in the one- and two-dimensional (1D and 2D) Anderson model. However, for three-dimensional (3D) case, an energy threshold, i.e., the mobility edge, appears in the single-particle spectrum and separates the ergodic eigenstates from the localized eigenstates. Beyond the Anderson-like model, the mobility edge appears in a class of generalized Aubry-André-Harper (AAH) models as well. It is known that there is no mobility edge in the standard AAH model [5–7], but the mobility edges can be induced by breaking the self-duality [8–12], such as introducing next-nearest-neighbor hopping [13], exponentially long-range hopping [8,14], off-diagonal incommensurate hopping [9,14–17], power law hopping [10,11,13,18], slowly varying potentials [19,20], and the generalized incommensurate potentials [17,21–27]. The studies on single-particle mobility edge [12,22,28–36] help us understand the roles that mobility edge plays on the thermalization and many-body localization in interacting quasidisordered extensions [37–39].

Recently, there has been growing interest in studying the mobility edges in a class of generalized AAH models with power law hoppings [10,11,13,40], which can be induced by power law interactions [13,40]. Deng *et al.* found that, when the power law index $a < 1$, there are ergodic-to-multifractal (EM) edges in the intermediate regimes, and when $a > 1$, there are ergodic-to-localized (EL) edges [10]. Particularly, the intermediate regimes are subdivided into P_ℓ regimes, where the fraction of the ergodic states are of β^ℓL (β is a quasiperiodic parameter measuring the member of the metallic mean family, L is the system size, and $\ell = 1, 2, 3, \ldots$). Roy and Sharma discussed the influence of the metallic mean family on the intermediate regime, and a generalized phase diagram based on the irrational diophantine numbers and their sequences are charted out [11]. Xu *et al.* studied the non-Hermitian effect on the power law hopping system [41] and found that the aforementioned P_ℓ regimes are destroyed by the non-Hermitian effect and the EM and EL edges are independent of the quasiperiodic parameter β. Besides, the localization transition points and the exact expression of the EL edge are derived, which are self-consistent with numerical results. In this work, we are motivated to study whether the β-dependent P_ℓ regimes are robust against the non-Hermitian transition effect. In addition, we will try to understand the absence of the localized states in the long-range hopping regime and analytically obtain the EL edges in the short-range hopping regime (such as $a = 2$).

The organization of the paper is as follows: In Sec. II, we describe the Hamiltonian of the non-Hermitian AAH model with power law hopping and introduce the metallic mean family. In Sec. III, we study the localization properties under the weak non-Hermitian effect. In Sec. IV, we study the localization properties under the strong non-Hermitian effect. We studied the relationship between the localization transition of the eigenstates and the breaking of the PT symmetry in the

*chensj@zjnu.edu.cn
†gaoxl@zjnu.edu.cn

case of both $a < 1$ and $a > 1$ in Sec. V. We summarize in Sec. VI.

II. MODEL AND HAMILTONIAN

A one-dimensional non-Hermitian AAH model that we considered consists of power law hoppings and complex on-site potentials and reads

$$H = -J \sum_{j,s} \frac{1}{s^a} (c_j^\dagger c_{j+s} + \text{H.c.}) + \sum_j \Delta_j c_j^\dagger c_j, \tag{1}$$

where J is set as the unit of energy, a is the power law index, J/s^a is the power law hopping strength between site j and site $j+s$, and $\Delta_j = \Delta \cos(2\pi\beta j + ik)$ denotes the non-Hermitian on-site potential. The non-Hermitian effect is introduced by an imaginary term ik. When $k = 0$, the model goes back to the Hermitian case [10,11], where EM edges are uncovered. Δ_j satisfies the relation $\Delta_{-j} = \Delta_j^*$, therefore the Hamiltonian H is PT symmetric [26,41]. β is chosen at the metallic mean family, which can be derived from a generalized u-Fibonacci recurrence relation $F_{v+1} = uF_v + F_{v-1}$ with $F_0 = 0$ and $F_1 = 1$. The golden mean $\beta = \beta_g$ is obtained by the limit $\beta_g = \lim_{v\to\infty} F_{v-1}/F_v$ when $u = 1$. Besides, this recurrence can yield another metallic mean, such as the silver mean $\beta = \beta_s = \sqrt{2} - 1$ when $u = 2$ and the bronze mean $\beta = \beta_b = (\sqrt{13} - 3)/2$ when $u = 3$. β_g and β_s will be used in following numerical calculations.

With the basis $|\psi_n\rangle = \sum_j \phi_j^n |j\rangle = \sum_j \phi_j^n c_j^\dagger |0\rangle$, we obtain the following eigenfunction:

$$-J \sum_s \frac{1}{s^a} (\phi_{j-s}^n + \phi_{j+s}^n) + \Delta_j \phi_j^n = E_n \phi_j^n, \tag{2}$$

where ϕ_j^n is the amplitude at the jth site of the nth wave function, and E_n is the corresponding eigenenergy. Here the eigenenergy levels with ascending order are sorted according to the real part of E_n.

III. LOCALIZATION PROPERTIES UNDER WEAK NON-HERMITIAN EFFECT

As mentioned before, the parameter k dominates the non-Hermitian effect. When k is small, the non-Hermitian effect is weak, whereas it is strong when k is large. In this section, we mainly study the weak non-Hermitian case with $k = 0.8$ and $\beta = \beta_g$. The phase diagram of the model in Eq. (1) with $\beta = \beta_g$ has been presented in Fig. 1. We find that the non-Hermitian system preserves similar features as the Hermitian one. For $a \gg 1$, we recover the non-Hermitian AAH model [26] with nearest-neighbor hoppings, and therefore all eigenstates are either ergodic (the purple regime with the fraction of ergodic eigenstates $\lambda = 1$) for $\Delta < 2e^{-k}J$ or localized (black regime with the fraction of ergodic eigenstates $\lambda = 0$) for $\Delta > 2e^{-k}J$ (see the derivation in Appendix A). As can be seen from the phase diagram in addition to ergodic (purple regime) and localized (black regime) phases with the fraction of ergodic eigenstates $\lambda = 1$ and $\lambda = 0$, respectively, there is an intermediate phase with $0 < \lambda < 1$. In particular, in the intermediate phase, there are four $P_{\ell=1,2,3,4}$ regimes where the lowest β^ℓL eigenstates are ergodic with fractions $\lambda = \beta_g$ (orange regime, marked by P_1), β_g^2 (red regime, marked by P_2), β_g^3 (blue regime, marked by P_3), and β_g^4 (green regime, marked by P_4). Compared with the Hermitian cases [10], the remarkable differences are reflected in the fact that the four regimes are suppressed by the non-Hermitian effect and are separated by the normal intermediate regimes, where the fraction of ergodic states are β independent. Meanwhile, the original $P_{\ell>4}$ regimes no longer exist. In the following, we clarify the similarities and differences between the P_ℓ regimes and the normal intermediate regime by investigating the fractal dimension.

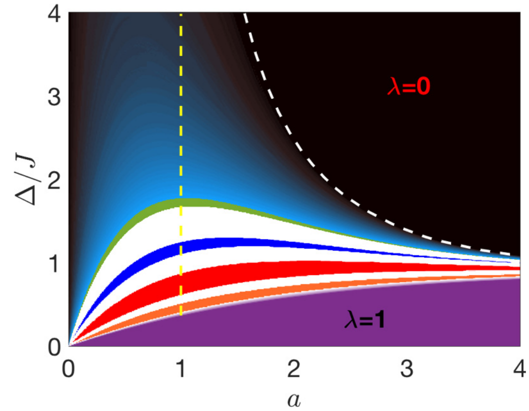

FIG. 1. The phase diagram of the non-Hermitian AAH model with power law hopping index a and the strength of the complex potential Δ for $\beta_g = 610/987$, $k = 0.8$ and the system size $L = 987$. In addition to ergodic (purple regime) and localized (black regime) phases with the fraction of ergodic eigenstates $\lambda = 1$ and $\lambda = 0$, respectively, there is an intermediate phase with $0 < \lambda < 1$. In particular, in the intermediate phase, there are four $P_{\ell=1,2,3,4}$ regimes with fractions $\lambda = \beta_g$ (orange regime, marked by P_1), β_g^2 (red regime, marked by P_2), β_g^3 (blue regime, marked by P_3), and β_g^4 (green regime, marked by P_4). The vertical yellow dashed line separates the long-range ($a < 1$) and short-range ($a > 1$) hopping cases. The white dashed line represents the boundary between the localized phase and the intermediate phase. The light blue and white regimes both represent the normal intermediate phase, where the fraction of ergodic eigenstates λ does not depend on the quasiperiodic parameter β. Meanwhile, the white regime can be viewed as a transition regime between two adjacent P_ℓ regimes.

The fractal dimension D_f is defined based on the box-counting procedure [42–45] and is expressed as

$$D_f = \lim_{L_d\to\infty} \frac{1}{1-f} \frac{\ln \sum_{m=1}^{L_d} (\mathcal{I}_m)^f}{\ln L_d}, \tag{3}$$

where $L_d = L/d$ is the number of the box with L being the system size and d being the box counting index, f is the scale index, and $\mathcal{I}_m = \sum_{j\in m} |\psi_n(j)|^2$ corresponds to the probability of detecting inside the mth box for the nth normalized eigenstate $|\psi_n(j)\rangle$. Without loss of generality, we study the fractal dimension D_2. Considering the system size $L = 2584$, and the box counting index $d = 4$, as well as the golden mean $\beta_g = 1597/2584$, we plot D_2 of full eigenstates as a function of the strength of the complex potential Δ for $a = 0.5$ (long-range hopping) in Fig. 2(a) and for $a = 2.0$ (short-range hopping) in Fig. 2(b), respectively. It is readily seen that, in

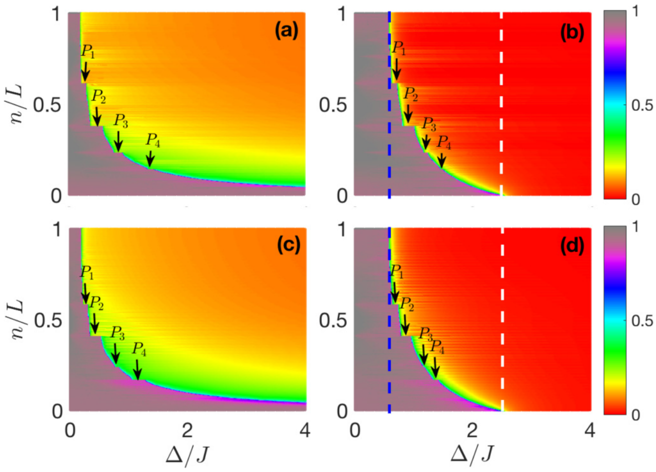

FIG. 2. Fractal dimension D_2 (shown in color) of different eigenstates as a function of Δ with $k = 0.8$, $L = 2584$, $d = 4$, and $\beta_g = 1597/2584$ for (a) $a = 0.5$ and (b) $a = 2$, and with $k = 0.8$, $L = 2378$, $d = 2$, and $\beta_s = 985/2378$ for (c) $a = 0.5$ and (d) $a = 2$. In panels (b) and (d), the blue and white dashed lines correspond to $\Delta_{c1} \approx 0.6J$ and $\Delta_{c2} \approx 2.4J$, respectively.

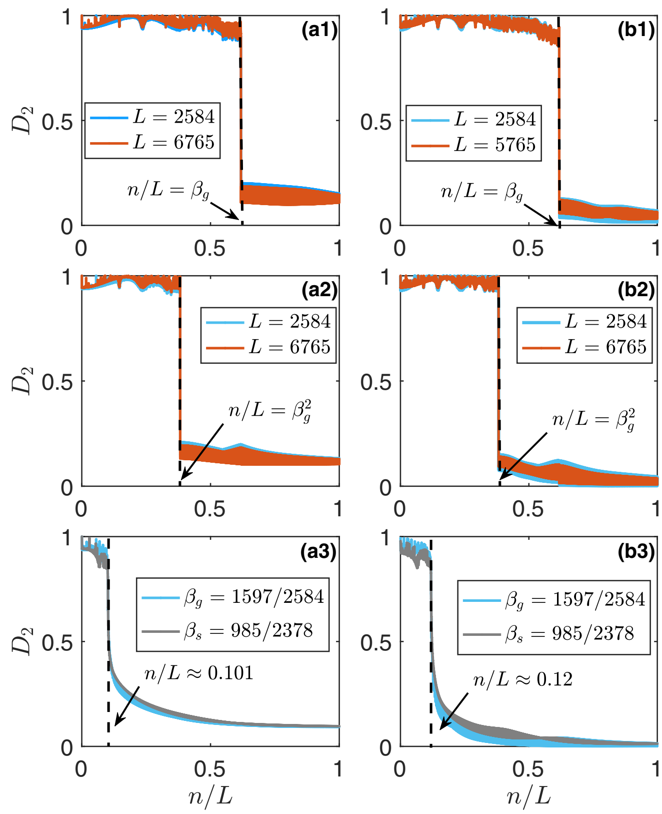

FIG. 3. (a1)–(a3) D_2 versus the index n/L for $k = 0.8$ and $a = 0.5$ with $\Delta = 0.3J$, $0.5J$, and $2J$, respectively. (b1)–(b3) D_2 versus the index n/L for $k = 0.8$ and $a = 2.0$ with $\Delta = 0.73$, 0.9, and 1.6, respectively. The dashed lines represent the energy indexes of the localization transitions. Here, for $L = 2584$, we take $\beta_g = 1597/2584$ and $d = 4$, and for $L = 6765$, we choose $\beta_g = 4181/6765$, $d = 5$, respectively. For $\beta_s = 985/2378$, we take $L = 2378$ and $d = 2$.

the $P_{\ell=1,2,3,4}$ regimes, two types of edges present a step-wise dependence on Δ, equaling $\lambda = \beta_g^\ell$. Out of the four regimes, λ smoothly changes as Δ increases. In fact, the absence of $P_{\ell>4}$ regimes is related to the non-Hermitian effect. When the complex phase disappears, the system returns to the Hermitian case, where there are complete P_ℓ regimes. As k increases, higher-P_ℓ regimes gradually vanish. When $k \to \infty$, there is no P_ℓ regime. The system with $k = 0.8$ is one of the intermediate cases within the two limits, which reflects that the lower P_ℓ regimes are robust against the weak non-Hermiticity. For other proper complex phases, we can see the similar results as well. In other words, when $k < 0.8$, we can observe more P_ℓ regimes (see the case of $k = 0.3$ in Appendix B).

In fact, similar phenomena appear in the $\beta = \beta_s$ case as well. For systems size $L = 2378$ and different box counting index $d = 2$, as well as the silver mean $\beta_s = 985/2378$, we plot D_2 as a function of Δ for $a = 0.5$ (long-range hopping) in Fig. 2(c) and for $a = 2.0$ (short-range hopping) in Fig. 2(d), respectively. Compared with Figs. 2(a) and 2(b), the two types of edges display a different step-wise dependence on the Δ in the $P_{\ell=1,2,3,4}$ regimes [$\lambda = \beta_s + \beta_s^2$ (P_1), β_s (P_2), $\beta_s^2 + \beta_s^3$ (P_3), $2\beta_s^3 + \beta_s^4$ (P_4), respectively] and a same smooth changing of λ out of the P_ℓ regimes still exist. It implies that the step-wise dependence on the Δ in the $P_{\ell=1,2,3,4}$ regimes depends on the quasiperiodic parameter β.

Next, we further study the different localization phenomena in the long-range hopping and the short-range hopping cases and the differences between the P_ℓ regimes and the normal intermediate regimes. We fix $L = 2584$ and $\beta_g = 1597/2584$ in the calculations. For the long-range hopping case ($a = 0.5$) and $\Delta = 0.3J$ chosen in the P_1 regime, we can see that, in Fig. 3(a1), below $n/L = \beta_g$, D_2 tends to 1, corresponding to the ergodic eigenstates, and above $n/L = \beta_g$, D_2 tends to a finite value, corresponding to the multifractal eigenstates. In this case, the abrupt change of D_2 from 1 to a nonzero value presents an EM transition at $n/L = \beta_g$. In contrast with the long-range case, we can see that, for short-range hopping [Fig. 3(b1)], D_2 changes from 1 to zero, showing an EL transition at $n/L = \beta_g$. For higher-P_ℓ regimes, the similar phenomena still exists. We take $\Delta = 0.5J$ and $\Delta = 0.9J$ from the P_2 regime, the corresponding D_2 for $a = 0.5$ and $a = 2$ are plotted in Figs. 3(a2) and 3(b2), respectively. The two diagrams present an EM transition and an EL transition at $n/L = \beta_g^2$, respectively. As shown in Figs. 3(a1), 3(a2), 3(b1), and 3(b2), we can see the fractal dimensions D_2 are independent of system size L. From the above analysis, we can see that, in the P_ℓ regimes, the two types of edges show dependence on β. In fact, the two types of transitions appear in the normal intermediate regimes as well [see the EM transition in Fig. 3(a3) and the EL transition in Fig. 3(b3), respectively], where the EL edge and EM edge are visibly β independent. Meanwhile, the results suggest that the features aroused by the hopping types (controlled by a) are robust against the weak non-Hermitian effect.

In the above analysis, we have used the special fractal dimension D_2 to determine the localization properties of the system. To further clarify the existence of multifractality in the regime $a < 1$, we plot the average of D_f over the target eigenstates, i.e., $\overline{D_f}$, as a function of f for the P_2 regime ($\lambda = \beta_g^2$) for $a = 0.5$ [in Fig. 4(a)] and $a = 2$ [in Fig. 4(b)]

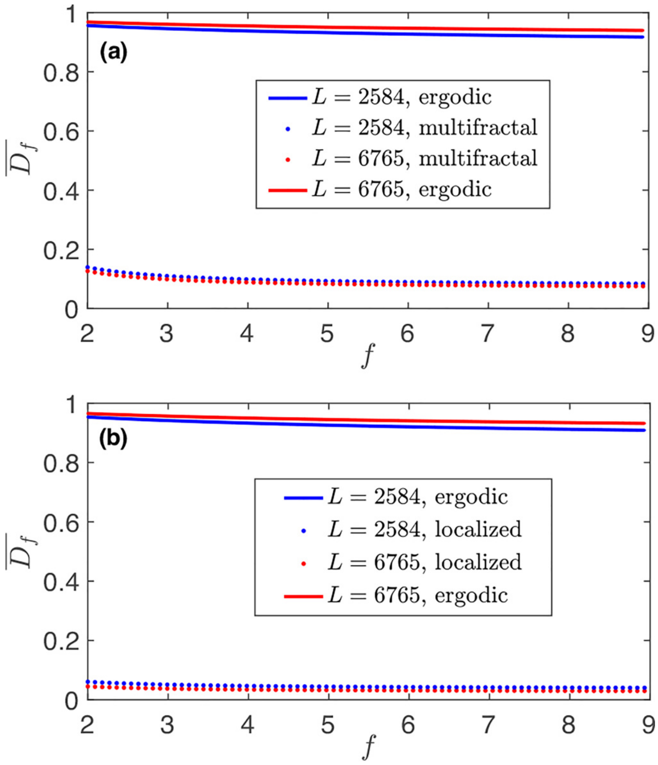

FIG. 4. (a) Averaged fractal dimension $\overline{D_f}$ as a function of f for $k = 0.8$, $\beta_g = 1597/2584$, $\Delta = 0.4J$, and $a = 0.5$ for the system in the P_2 regime with an EM edge. (b) Averaged fractal dimension $\overline{D_f}$ as a function of f for $k = 0.8$, $\beta_g = 1597/2584$, $\Delta = 0.9J$, and $a = 2$ for the system in the P_2 regime with an EL edge. $\overline{D_f}$ is calculated by averaging over β_g^2 fraction of ergodic states and $(1-\beta_g^2)$ fraction of multifractal or localized states. Here, for $L = 2584$, we take $\beta_g = 1597/2584$ and $d = 4$, and for $L = 6765$, we take $\beta_g = 4181/6765$, $d = 5$.

in the system with $\beta = \beta_g$. In Figs. 4(a) and 4(b), $\overline{D_f}$ shown with the solid red and blue curves are the average of D_f over the lowest $\beta_g^2 L$ eigenstates and are close to 1 for different f, indicating the ergodic states, and are almost independent of the system sizes. $\overline{D_f}$ shown with the blue and red dashed curves are the average of D_f over the highest $(1-\beta_g^2)L$ eigenstates. Intuitively, for various f and system sizes, $\overline{D_f}$ show a weak dependence on f for $a = 0.5$, whereas $\overline{D_f}$ approach to 0 and is almost independent of f for $a = 2$. It indicates that these eigenstates are multifractal for $a = 0.5$ and localized for $a = 2$.

Now we first discuss the absence of localized states for $a < 1$. After performing the Fourier transformation $g(\tilde{\theta}) = \frac{1}{\sqrt{L}}\sum_j \phi_j e^{i\tilde{\theta} j}$ where $\tilde{\theta} = 2\pi\theta$, we have the following dual equation of Eq. (2):

$$\frac{\Delta e^{k}}{2} g(\tilde{\theta} - \tilde{\omega}) + \frac{\Delta e^{-k}}{2} g(\tilde{\theta} + \tilde{\omega}) = \left(E + \sum_s \frac{2}{s^a}\cos(s\tilde{\theta})\right) g(\tilde{\theta}), \quad (4)$$

where $\tilde{\omega} = 2\pi\beta$ and the index n has been suppressed. For $a < 1$, the dual potential $\sum_s 2\cos(s\tilde{\theta})/s^a$ is divergent. According to Simon-Spencer theorem [46,47] and its application [41], the spectrum E of the dual eigenfunction is not absolutely continuous. Thus, for our model, there is no localized state in the $0 < a < 1$ regime.

Next, we analyze the location of the intermediate regime and the critical point of the EL transition for $a > 1$. Here, we take $a = 2$ as a specific example. According to the Avila's global theory [48] and its application [49], we first make an analytical continuation on Δ_j, i.e., $ik \to i(k+\delta)$. Thus, in the limit $\delta \to \infty$, the dual equation in Eq. (4) reduces to

$$\frac{\Delta e^{k+\delta}}{2} g(\tilde{\theta} - \tilde{\omega}) = \left(E + \sum_s \frac{2}{s^a}\cos(s\tilde{\theta})\right) g(\tilde{\theta}). \quad (5)$$

Reference [41] tells us that we can analytically extract the localization properties when the analytical continuation δ recovers to zero. Meanwhile, the infinite series $\sum_s 2\cos(s\tilde{\theta})/s^2$ converges to $\tilde{\theta}^2/2 - \pi\tilde{\theta} + \pi^2/3$ [41]. Therefore, we finally obtain the following dual equation

$$\frac{\Delta e^{k}}{2} g(\tilde{\theta} - \tilde{\omega}) = (E + \tilde{\theta}^2/2 - \pi\tilde{\theta} + \pi^2/3) g(\tilde{\theta}). \quad (6)$$

The Sarnak method [50] and its application [51] tells us that the location of the intermediate regime and the EL edge are related to the following characteristic function:

$$\begin{aligned} G(E) &= \frac{1}{2\pi}\int_0^{2\pi} \ln\left|E + \frac{\tilde{\theta}^2}{2} - \pi\tilde{\theta} + \frac{\pi^2}{3}\right| \\ &= -\ln 2 + \frac{1}{2\pi}\int_0^{2\pi} \ln\left|(\tilde{\theta} - \pi)^2 - \left(\frac{\pi^2}{3} - 2E\right)\right| \\ &= -2 - \ln 2 + \frac{\epsilon_+ \ln\epsilon_+ + \epsilon_- \ln\epsilon_-}{\pi}, \end{aligned} \quad (7)$$

where $\epsilon_\pm = \pi \pm (\pi^2/3 - 2E)^{1/2}$. By $\{G(E) > \ln|\frac{\Delta e^k}{2}|\} \cap \epsilon_E$, where the set of spectrum $\epsilon_E = [-\pi^2/3, \pi^2/6]$ guarantees the existence of the solution to the equation $E + \tilde{\theta}^2/2 - \pi\tilde{\theta} + \pi^2/3 = 0$ with E being a real value, we can locate the intermediate regime. Within ϵ_E, we have $G \in [2\ln\pi - \ln 2 - 2, 2\ln\pi + \ln 2 - 2]$. Therefore, the lower bound of the intermediate regime satisfies $\Delta_{c1} = 2e^{-k}e^{2\ln\pi - \ln 2 - 2}$, and the upper bound satisfies $\Delta_{c2} = 2e^{-k}e^{2\ln\pi + \ln 2 - 2}$. When $\Delta < \Delta_{c1}$, all the eigenstates are ergodic, and when $\Delta > \Delta_{c2}$, all the eigenstates are localized. From the expressions of Δ_{c1} and Δ_{c1}, we can see that the bounds Δ_{c1} and Δ_{c1} exponentially decay with the increase of the non-Hermiticity strength k, which means that the ergodic phase will vanish when $k \to \infty$. For the $k = 0.8$ case, $\Delta_{c1} \approx 0.6J$ and $\Delta_{c2} \approx 2.4J$, which are shown in Figs. 2(b) and 2(d), labeled by blue and white dashed lines, respectively.

IV. THE LOCALIZATION PROPERTIES UNDER THE STRONG NON-HERMITIAN EFFECT

In this section, we study the localization properties under the strong non-Hermitian effect with $k = 3$. We find that the long-range-hopping-induced EM edges and the short-range-hopping-induced EL edges are robust against the strong non-Hermitian effect, but the β-dependent P_ℓ regimes disappear completely. Meanwhile, the fractions of the EM and EL edges are completely independent of the value of β. To study

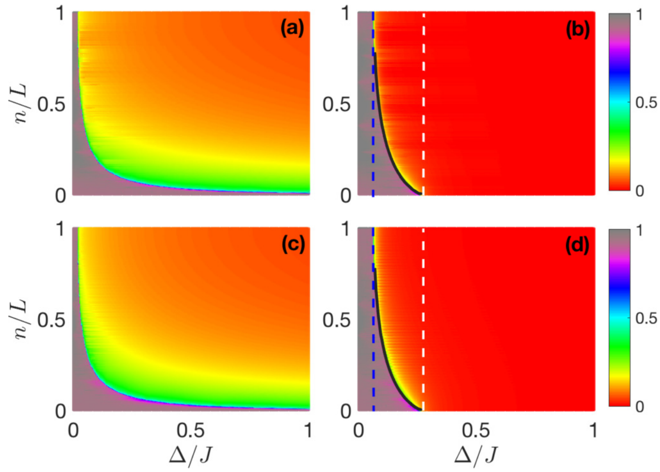

FIG. 5. Fractal dimension D_2 (shown in color) of different eigenstates as a function of the strength of the complex potential Δ with $k = 3$, $L = 2584$, $d = 4$, and $\beta_g = 1597/2584$ for (a) $a = 0.5$ and (b) $a = 2$, and with $k = 3$, $L = 2378$, $d = 2$, and $\beta_s = 985/2378$ for (c) $a = 0.5$ and (d) $a = 2$. In panels (b) and (d), the blue and white dashed lines satisfy $\Delta_{c1} \approx 0.066J$ and $\Delta_{c2} \approx 0.266J$, respectively, and the black solid lines represent the EL edges E_c determined by $G(E_c) = \ln|\frac{\Delta e^k}{2}|$.

the localization properties under the strong non-Hermitian effect with $k = 3$, we calculate the fractal dimension D_2 of different eigenstates as a function of Δ. As shown in Figs. 5(a) and 5(c), for $a = 0.5$, no matter β is $\beta_g = 1597/2584$ or $\beta_s = 985/2378$, the EM edge smoothly decreases as Δ increases, and the EM edges are β independent. As shown in Figs. 5(b) and 5(d), for $a = 2$, no matter β is $\beta_g = 1597/2584$ or $\beta_s = 985/2378$, the EL edges smoothly decay with the increase of Δ and is independent of β, too. In addition, the bounds of the intermediate regime for the short-range hopping case ($a = 2$) can be analytically obtained as well. Employing the same analytical methods as those done for the $k = 0.8$ case, here the lower bound of the intermediate regime satisfies $\Delta_{c1} \approx 0.066J$ and the upper bound satisfies $\Delta_{c2} \approx 0.266J$, which are shown in Figs. 5(b) and 5(d), labeled by blue and white dashed lines, respectively. Meanwhile, according to the above-mentioned Sarnak method, the critical point E_c of the EL transition can be determined by $G(E_c) = \ln|\frac{\Delta e^k}{2}|$, which are labeled by the black solid lines in Figs. 5(b) and 5(d).

To further explain the β-independent features, we calculate single-parameter D_2 curves for two different quasiperiodic parameters β. For $a = 0.5$, Fig. 6(a) shows that, when β are taken as $\beta_g = 1597/2584$ and $\beta_s = 985/2378$, the fractal dimensions D_2 both jump at $n/L \approx 0.201$ under the same parameter $a = 2$ and $\Delta = 0.1J$. When $n/L < 0.201$, the corresponding eigenstates are ergodic with $D_2 \approx 1$. For $n/L > 0.201$, the corresponding eigenstates show the multifractal feature with D_2 being finite values. This indicates that there are same EM edges at $n/L \approx 0.201$ for different β. As shown in Fig. 6(b), no matter β is equal to $\beta_g = 1597/2584$ or equal to $\beta_s = 985/2378$, the fractal dimension D_2 under $k = 3$, $\Delta = 0.11J$, and $a = 2$ both jump from $D_2 \to 1$ to $D_2 \to 0$ at $n/L \approx 0.322$. This indicates that there are the same EL edges at $n/L \approx 0.322$ for different β.

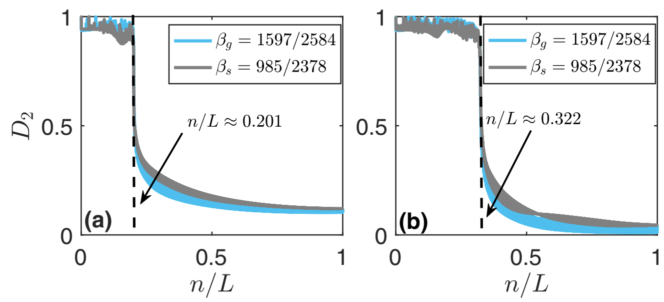

FIG. 6. D_2 versus the index n/L with different β and $k = 3$. (a) $a = 0.5$ and $\Delta = 0.1J$. (b) $a = 2$ and $\Delta = 0.11J$. The dashed lines represent the energy indexes of the localization transitions Here, for $\beta_g = 1597/2584$, we take $L = 2584$, $d = 4$, and for $\beta_s = 985/2378$, we take $L = 2378$ and $d = 2$.

V. *PT* SYMMETRY BREAKING

Next, we study the *PT* symmetry breaking in the cases of $a < 1$ and $a > 1$. Figures 7(a) and 7(b) present the behavior of the maximum value of $|\mathrm{Im}(E)|$ and the fractal dimension $D_2(L)$ of the Lth eigenstate as a function of Δ for $a = 0.5$ and $a = 2$, respectively. As can be seen from Fig. 7(a), the *PT* symmetry-breaking point coincides with the EM phase transition point at $\Delta \approx 0.21J$ for $a = 0.5$ and coincides with the EL phase-transition point at $\Delta \approx 0.6J$ for $a = 2$ [in Fig. 7(b)]. The energy spectrum for $\Delta = 0.1J$ and $\Delta = 0.4J$ are shown in Figs. 8(a) and 8(b), respectively, where all the eigenvalues are real. In the intermediate regime, the complex energies emerge. As shown in Fig. 8(c) with $a = 0.5$ and $\Delta = 0.5J$, the real-complex transition of the energy spectrum is synchronized with the EM transition [see Fig. 3(a2)]. Besides, we can see that in Fig. 8(d) with $a = 2$ and $\Delta = 0.9J$, there exist the

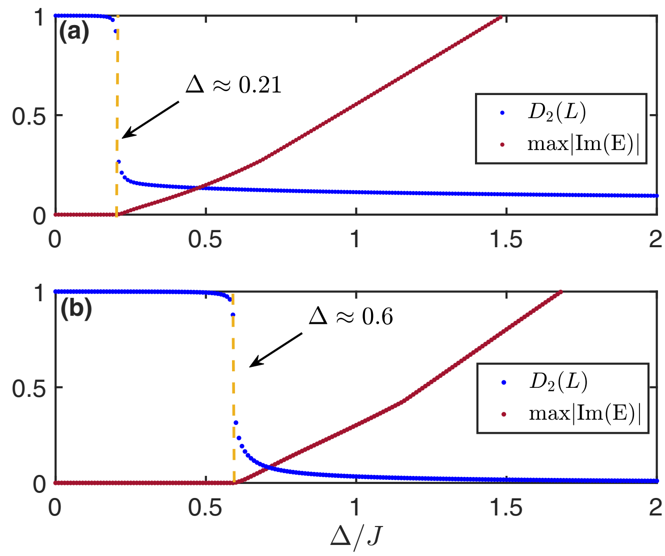

FIG. 7. The behavior of the maximum value of |Im(E)| and the fractal dimension of the Lth eigenstate $D_2(L)$ as the functions of Δ with $k = 0.8$, $\beta_g = 1597/2584$, and $L = 2584$ for (a) $a = 0.5$ and (b) $a = 2$, respectively. The dashed lines denote the *PT* symmetry-breaking point and the EM transition point in panel (a) and EL transition point in panel (b), respectively.

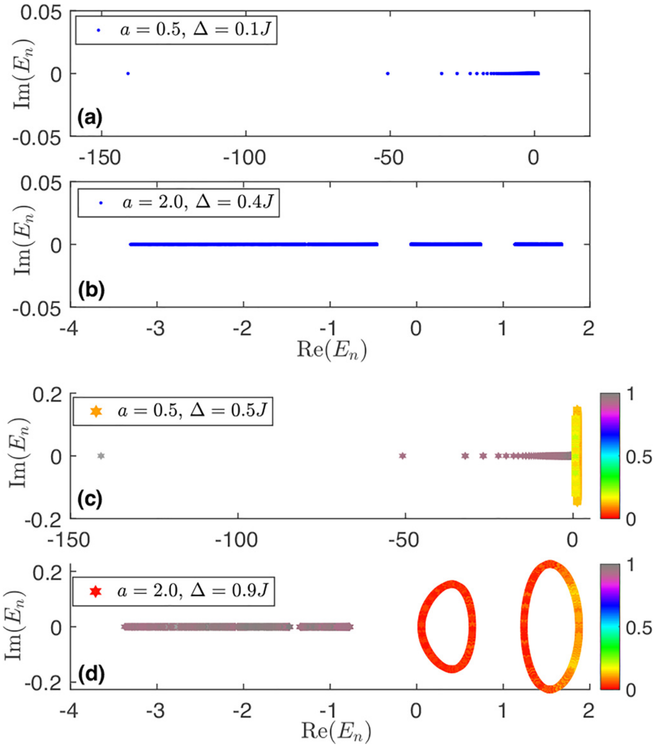

FIG. 8. Energy spectrum E_n with $L = 2584$, $k = 0.8$, and $\beta_g = 1597/2584$ for (a) $\Delta = 0.1J$, $a = 0.5$, (b) $\Delta = 0.4J$, $a = 2$, (c) $a = 0.5$, $\Delta = 0.5J$, and (d) $a = 2$, $\Delta = 0.9J$, respectively. The color bar shows the value of fractal dimension D_2.

real-complex transition of the energy spectrum accompanied by the EL transition [see Fig. 3(b2)].

VI. CONCLUSION

In conclusion, a non-Hermitian AAH model with power law hoppings was studied. We uncover that the quasiperiodic parameter β-dependent P_ℓ regimes are robust against the weak non-Hermitian effect. When the non-Hermitian effect gets stronger, the P_ℓ regimes disappear. However, we find that localization properties, i.e., the long-range hopping induced EM edge and the short-range hopping induced EL edge are robust against the non-Hermitian effect and are well characterized by the fractal dimension D_2. We argued that the absence of the localized states for the long-range hopping case by the Simon-Spencer theorem. Meanwhile, by employing the Sarnak method and Avila's global theory, the boundaries of the intermediate regime and the critical points of the EL phase transition for the short-range hopping case ($a = 2$) are analytically located, which are coincident with the numerical results. Finally, we analyzed the relationship between the PT symmetry breaking and the EM and EL phase transitions. We found that the ergodic eigenstates correspond to the real eigenenergies, whereas the multifractal and localized eigenstates correspond to the complex eigenenergies.

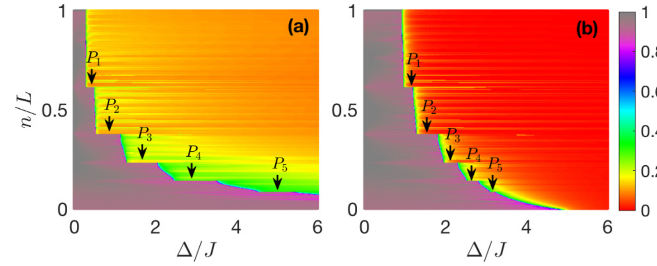

FIG. 9. Fractal dimension D_2 (shown in color) of different eigenstates as a function of Δ with $k = 0.3$, $L = 2584$, $d = 4$, and $\beta_g = 1597/2584$ for (a) $a = 0.5$ and (b) $a = 2$, respectively.

ACKNOWLEDGMENTS

The authors acknowledge support from NSFC under Grants No. 11835011 and No. 12174346.

APPENDIX A: THE DERIVATION OF THE PHASE BOUNDARY IN THE LIMIT CASE $a \gg 1$

When $a \gg 1$, the Schrödinger equation can be rewritten in the following transfer-matrix form:

$$\begin{pmatrix} \phi_{j+1} \\ \phi_j \end{pmatrix} = T_j \begin{pmatrix} \phi_j \\ \phi_{j-1} \end{pmatrix}, \tag{A1}$$

with

$$T_j = \begin{pmatrix} \frac{V\cos(2\pi\alpha j + ik) - E}{J} & -1 \\ 1 & 0 \end{pmatrix}. \tag{A2}$$

Accordingly, the Lyapunov exponent γ can be obtained by

$$\gamma = \lim_{L\to\infty} \frac{1}{L} \ln \left\| \prod_{j=1}^{L} T_j \right\|. \tag{A3}$$

We derive γ by employing the Avila's global theory [48]. According to this theory, an analytical continuation on the phase is necessary, i.e., $ik \to ik + i\epsilon$. In the limit $\epsilon \to \infty$, we have

$$T_j = e^{-i2\pi\alpha j + \delta} \begin{pmatrix} \frac{Ve^k}{2J} & 0 \\ 0 & 0 \end{pmatrix}, \tag{A4}$$

which yields $\gamma_{\epsilon\to\infty} = |\epsilon| + \max\{\ln|Ve^k/2J|, 0\}$. According to this Avila's global theory, the Lyapunov exponent of the system is determined when ϵ returns to zero, namely

$$\gamma_{\epsilon=0} = \max\{\ln|Ve^k/2J|, 0\}. \tag{A5}$$

Therefore, the phase boundary V_c is determined by $\ln|V_c e^k/2J| = 0$, i.e., $V_c = 2e^{-k}J$.

APPENDIX B: THE CASE OF $k = 0.3$

When $k = 0.3$, as shown in Fig. 9, we can observe the P_5 regime.

[1] P. W. Anderson, Absence of diffusion in certain random lattices, Phys. Rev. **109**, 1492 (1958).

[2] E. Abrahams, P. W. Anderson, D. C. Licciardello, and T. V. Ramakrishnan, Scaling Theory of Localization: Absence of

Quantum Diffusion in Two Dimensions, Phys. Rev. Lett. **42**, 673 (1979).

[3] Y. Lahini, A. Avidan, F. Pozzi, M. Sorel, R. Morandotti, D. N. Christodoulides, and Y. Silberberg, Anderson Localization and Nonlinearity in One-Dimensional Disordered Photonic Lattices, Phys. Rev. Lett. **100**, 013906 (2008).

[4] Y. Lahini, Y. Bromberg, D. N. Christodoulides, and Y. Silberberg, Quantum Correlations in Two-Particle Anderson Localization, Phys. Rev. Lett. **105**, 163905 (2010).

[5] S. Aubry and G. André, Analyticity breaking and Anderson localization in incommensurate lattices, Ann. Israel Phys. Soc. **3**, 18 (1980).

[6] I. M. Suslov, Localization in one-dimensional incommensurate systems, Sov. J. Exp. Theor. Phys. **56**, 612 (1982).

[7] M. Wilkinson, Critical properties of electron eigenstates in incommensurate systems, Proc. R. Soc. London, Ser. A **391**, 305 (1984).

[8] J. Biddle and S. Das Sarma, Predicted Mobility Edges in One-Dimensional Incommensurate Optical Lattices: An Exactly Solvable Model of Anderson Localization, Phys. Rev. Lett. **104**, 070601 (2010).

[9] W. Chen, S. Cheng, J. Lin, R. Asgari, and G. Xianlong, Breakdown of the correspondence between the real-complex and delocalization-localization transitions in non-Hermitian quasicrystals, Phys. Rev. B **106**, 144208 (2022).

[10] X. Deng, S. Ray, S. Sinha, G. V. Shlyapnikov, and L. Santos, One-Dimensional Quasicrystals with Power-Law Hopping, Phys. Rev. Lett. **123**, 025301 (2019).

[11] N. Roy and A. Sharma, Fraction of delocalized eigenstates in the long-range Aubry-André-Harper model, Phys. Rev. B **103**, 075124 (2021).

[12] T. Liu, H. Guo, Y. Pu, and S. Longhi, Generalized Aubry-André self-duality and mobility edges in non-Hermitian quasiperiodic lattices, Phys. Rev. B **102**, 024205 (2020).

[13] J. Biddle, D. J. Priour, B. Wang, and S. Das Sarma, Localization in one-dimensional lattices with non-nearest-neighbor hopping: Generalized Anderson and Aubry-André models, Phys. Rev. B **83**, 075105 (2011).

[14] Y. Liu, Y. Wang, Z. Zheng, and S. Chen, Exact non-Hermitian mobility edges in one-dimensional quasicrystal lattice with exponentially decaying hopping and its dual lattice, Phys. Rev. B **103**, 134208 (2021).

[15] C.-X. Guo, C.-H. Liu, X.-M. Zhao, Y. Liu, and S. Chen, Exact Solution of Non-Hermitian Systems with Generalized Boundary Conditions: Size-Dependent Boundary Effect and Fragility of the Skin Effect, Phys. Rev. Lett. **127**, 116801 (2021).

[16] Y. Liu, Y. Zeng, L. Li, and S. Chen, Exact solution of the single impurity problem in nonreciprocal lattices: Impurity-induced size-dependent non-Hermitian skin effect, Phys. Rev. B **104**, 085401 (2021).

[17] Y. Liu, Y. Wang, X.-J. Liu, Q. Zhou, and S. Chen, Exact mobility edges, $\mathcal{PT}$-symmetry breaking, and skin effect in one-dimensional non-Hermitian quasicrystals, Phys. Rev. B **103**, 014203 (2021).

[18] M. Saha, S. K. Maiti, and A. Purkayastha, Anomalous transport through algebraically localized states in one dimension, Phys. Rev. B **100**, 174201 (2019).

[19] S. Cheng and G. Xianlong, Majorana zero modes, unconventional real–complex transition, and mobility edges in a one-dimensional non-Hermitian quasi-periodic lattice, Chin. Phys. B **31**, 017401 (2022).

[20] S. Li, M. Li, Y. Gao, and P. Tong, Topological properties and localization transition in a one-dimensional non-Hermitian lattice with a slowly varying potential, Phys. Rev. B **105**, 104201 (2022).

[21] R. Farchioni, G. Grosso, and G. P. Parravicini, Incommensurate potentials: Analytic and numerical progress, J. Phys.: Condens. Matter **5**, B13 (1993).

[22] X. Li and S. Das Sarma, Mobility edge and intermediate phase in one-dimensional incommensurate lattice potentials, Phys. Rev. B **101**, 064203 (2020).

[23] C. Yuce, $\mathcal{PT}$ symmetric Aubry–André model, Phys. Lett. A **378**, 2024 (2014).

[24] Q.-B. Zeng, S. Chen, and R. Lü, Anderson localization in the non-Hermitian Aubry-André-Harper model with physical gain and loss, Phys. Rev. A **95**, 062118 (2017).

[25] H. Jiang, L.-J. Lang, C. Yang, S.-L. Zhu, and S. Chen, Interplay of non-Hermitian skin effects and Anderson localization in nonreciprocal quasiperiodic lattices, Phys. Rev. B **100**, 054301 (2019).

[26] S. Longhi, Topological Phase Transition in non-Hermitian Quasicrystals, Phys. Rev. Lett. **122**, 237601 (2019).

[27] Q.-B. Zeng and Y. Xu, Winding numbers and generalized mobility edges in non-Hermitian systems, Phys. Rev. Res. **2**, 033052 (2020).

[28] C. A. Müller, D. Delande, and B. Shapiro, Critical dynamics at the Anderson localization mobility edge, Phys. Rev. A **94**, 033615 (2016).

[29] C. M. Dai, W. Wang, and X. X. Yi, Dynamical localization-delocalization crossover in the Aubry-André-Harper model, Phys. Rev. A **98**, 013635 (2018).

[30] P. Qin, C. Yin, and S. Chen, Dynamical Anderson transition in one-dimensional periodically kicked incommensurate lattices, Phys. Rev. B **90**, 054303 (2014).

[31] R. Nilanjan and S. Auditya, Entanglement entropy and out-of-time-order correlator in the long-range Aubry–André–Harper model, J. Phys.: Condens. Matter **33**, 334001 (2021).

[32] X. Li, X. Li, and S. Das Sarma, Mobility edges in one-dimensional bichromatic incommensurate potentials, Phys. Rev. B **96**, 085119 (2017).

[33] S. Weidemann, M. Kremer, S. Longhi, and A. Szameit, Topological triple phase transition in non-Hermitian Floquet quasicrystals, Nature (London) **601**, 354 (2022).

[34] S. Longhi, Spectral deformations in non-Hermitian lattices with disorder and skin effect: A solvable model, Phys. Rev. B **103**, 144202 (2021).

[35] L.-Z. Tang, S.-N. Liu, G.-Q. Zhang, and D.-W. Zhang, Topological Anderson insulators with different bulk states in quasiperiodic chains, Phys. Rev. A **105**, 063327 (2022).

[36] S. Mu, L. Zhou, L. Li, and J. Gong, Non-Hermitian pseudo mobility edge in a coupled chain system, Phys. Rev. B **105**, 205402 (2022).

[37] K. Huang, D. Vu, X. Li, and S. Das Sarma, Incommensurate many-body localization in the presence of long-range hopping and single-particle mobility edge, Phys. Rev. B **107**, 035129 (2023).

[38] P. Bordia, H. Lüschen, U. Schneider, M. Knap, and I. Bloch, Periodically driving a many-body localized quantum system, Nat. Phys. **13**, 460 (2017).

[39] R. Hamazaki, K. Kawabata, and M. Ueda, Non-Hermitian Many-Body Localization, Phys. Rev. Lett. **123**, 090603 (2019).

[40] H. P. Lüschen, S. Scherg, T. Kohlert, M. Schreiber, P. Bordia, X. Li, S. Das Sarma, and I. Bloch, Single-Particle Mobility Edge in a One-Dimensional Quasiperiodic Optical Lattice, Phys. Rev. Lett. **120**, 160404 (2018).

[41] Z. Xu, X. Xia, and S. Chen, Non-Hermitian Aubry-André model with power-law hopping, Phys. Rev. B **104**, 224204 (2021).

[42] A. Chhabra and R. V. Jensen, Direct Determination of the f(α) Singularity Spectrum, Phys. Rev. Lett. **62**, 1327 (1989).

[43] M. Janssen, Multifractal analysis of broadly-distributed observables at criticality, Int. J. Mod. Phys. B **08**, 943 (1994).

[44] B. Huckestein, Scaling theory of the integer quantum Hall effect, Rev. Mod. Phys. **67**, 357 (1995).

[45] E. Cuevas, Multifractality of Hamiltonians with power-law transfer terms, Phys. Rev. B **68**, 184206 (2003).

[46] B. Simon and T. Spencer, Trace class perturbations and the absence of absolutely continuous spectra, Commun. Math. Phys. **125**, 113 (1989).

[47] B. Simon, *Trace Ideals and Their Applications*, 2nd ed. (American Mathematical Society, Rhode Island, 2005), p. 120.

[48] A. Avila, Global theory of one-frequency Schrödinger operators, Acta Math. **215**, 1 (2015).

[49] X. Cai and Y.-C. Yu, Exact mobility edges in quasiperiodic systems without self-duality, J. Phys.: Condens. Matter **35**, 035602 (2023).

[50] P. Sarnak, Spectral behavior of quasi periodic potentials, Commun. Math. Phys. **84**, 377 (1982).

[51] Z.-H. Xu, X. Xia, and S. Chen, Exact mobility edges and topological phase transition in two-dimensional non-Hermitian quasicrystals, Sci. China Math. **65**, 227211 (2022).